HIL Emulation for Future Aerospace Propulsion Systems

C. Gan, R. Todd, J. Apsley

School of Electrical and Electronic Engineering, The University of Manchester, UK
chengwei.gan@student.manchester.ac.uk

Keywords: Hardware-in-the-loop (HIL), mechanical system emulation, electrical drive, variable inertia, drivetrain, resonant mode

Abstract

Future transportation systems for aircraft, vehicles or marine vessels are all candidates for redesigned propulsion systems as a result of the more-electric revolution. Accurately emulating these new propulsion system designs to assess the dynamic engine-generator-electrical system interactions will be an invaluable design tool. A HIL mechanical emulation system is presented which utilises a novel compensator design to extend the emulation capability of a physical hardware system without the need for any hardware changes. A 30 kW test system is used to emulate variable inertia mechanical systems and drivetrain models to show the capability of a single test system to be used to emulate a wide range of systems. The compensator is not restricted to transport applications and will also improve the emulation of smartgrid sources and advanced renewable sources.

1 Introduction

The more-electric-aircraft (MEA) concept, or hybrid systems for vehicles or marine vessels, offer the opportunity to redesign the propulsion system to achieve significant environmental and platform-level benefits. For a MEA a single electric power off-take is necessary from the engine for non-propulsive power which enables a bleedless engine design [1] and also removes the need for a mechanical off-take shaft. Hybrid systems use a mix of electric propulsion and a smaller internal combustion engine. The development time and cost for a new engine design is massive, and given the potential for engine-generator-electrical system interactions due to their tightly integrated design, the overall system performance must be carefully evaluated throughout the design process.

Hardware-in-the-loop (HIL) techniques are widely used in power electronics and power system to replicate the behaviour of diverse systems [2, 3, 4]. In the case of mechanical power source emulation, the complex prime mover system can be accurately emulated by a HIL emulation system to allow the coupled power hardware, for example an electrical generator to be tested repeatedly, safely, and economically under a variety of realistic conditions. Modern HIL emulation systems consist of a commercial electrical drive system which acts as the emulator, and the emulated mechanical system is simulated on a real-time-platform (RTP) which sets the operating condition of the drive.

HIL prime mover emulation using an electrical drive is very common in transportation [5] and renewable applications [6]. In [5], a PI speed controller was designed to allow the shaft dynamics of a twin-shaft gas engine to be reproduced with a synchronous motor. [6] proposed a novel control structure for a wind turbine simulator in which two closed-loop controllers, a speed and torque control, are applied to the inverter-controlled induction motor. Since the electrical drive system has faster dynamics than the conventional mechanical system at the same power rating, the dynamic emulation of a high inertia mechanical power source using the electrical drives is relatively straightforward. However, when the inertia of the emulated application is smaller than the machine drive system, the emulation performance is limited. [7] presented a model-based control method for emulating an aeroderivative twin-shaft engine which has a 10 times smaller inertia in comparison with the machine of the same power rating. Some emulation limitations are evident in [7] resulting from accuracy and stability issues.

Mechanical drivetrains are widely used in hybrid vehicles to transmit power between the source and the electrical generator. Recently, most of the literature [8, 9] has been focused on the emulation of wind turbine drivetrains. [8] presents the use of a PWM DC-DC converter in the torque control of a DC motor where a hysteresis current control structure was implemented. The study in [8] shows some interesting emulation results of the harmonic torque, which is due to the gradient and tower shadow effects, through the measured armature current. However, the emulator is torque-controlled, which normally has a wider bandwidth in comparison to a speed loop control. In addition, the emulation accuracy on the torque oscillations is not given and only the speed variations due to the torque harmonics are presented with no comparison to the reference. In [9], a PI controller is designed using the frequency response method to replicate the drivetrain resonant modes of a wind turbine. However, due to the narrow bandwidth of the PI controller, the reproduction of the emulated resonant frequencies is not achieved.

This paper demonstrates a new compensator to cancel the natural dynamics of the electrical drive, which can allow the HIL emulation of high power and high speed mechanical power source systems by effectively extending the system

emulation bandwidth without any change to the actual hardware. The emulation performance of a simple variable inertia system and a simplified mechanical drivetrain are evaluated, as these systems represent the fundamental behaviour of future propulsion systems which are anticipated to pose a challenge to existing emulation facilities.

2 Experimental Test Facility

Fig. 1 shows the emulation hardware [4], which consists of a dSPACE real-time platform (RTP) containing the mechanical system model, and a 115kW commercial vector controlled induction machine (IM) drive. The mechanical system model in the RTP receives the measured electrical generator torque, T_{Gen} on the common shaft, and external references as inputs. The RTP then outputs the speed reference from the mechanical system model to the speed-controlled electrical drive system.

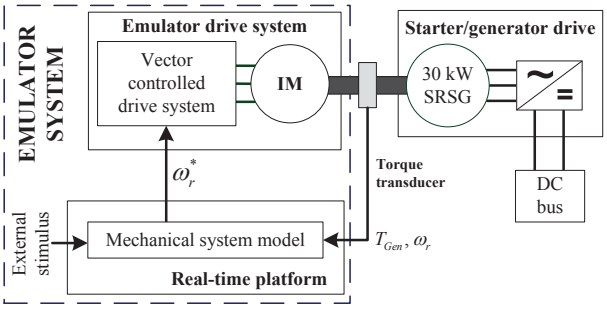

Figure 1. Block diagram of the emulation test facility.

A 30kW, 15,000rpm switched reluctance starter generator (SRSG) is connected to the emulator drive system. The generator is loaded using active load systems and resistive load banks which are connected to the generator through a reconfigurable DC network.

3 Proposed Emulation Compensator

Fig. 2 shows the control structure of the emulation drive system, where G_S is the speed controller of the drive system, G_P represents the rotor dynamics of the test rig, K_T is the drive torque constant, λ is a field weakening scaling and G_{comp} is the compensator for cancelling the mechanical characteristics of the electrical drive system. Transfer function parameters are listed in the Appendix.

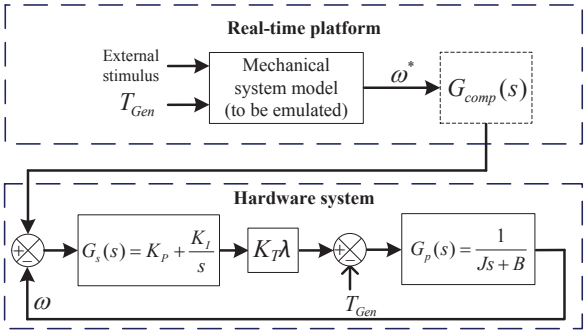

Figure 2. Block diagram of the compensator implementation.

The speed control loop dynamics compensator can be determined analytically [10] using the theoretical transfer function of the speed controller, providing the parameters are known and there is no variation in response with operating point. However, not all of the system parameters in Fig. 2 are known, more specifically communication and microcontroller delays, and ADC/DAC conversion circuits are unknown, so the analytical compensator method is not suitable.

In order to derive a better feedforward compensator without the requirement of accurate knowledge of the system parameters, an experimental system identification approach is applied to the system step response of the test rig [11]. The system identified transfer function in the continuous domain (identified from a 500rpm speed step test from 1000rpm to 1500rpm) is:

$$G_{TF} = \frac{16s + 1569}{s^2 + 17s + 1569} \tag{1}$$

The model order in (1) corresponds to that of the analytical system structure, (2) which is derived from Fig 2, and gives an excellent model fit performance in both the time and frequency domain, up to a bandwidth of approximate 100rad/s [11]. Extensive testing [11] has demonstrated that the effect of the electrical power load on the test rig dynamics is minor and so can be neglected over the frequency range offered by the compensator. The system dynamics have a noticeable difference at operating speeds above the machine base speed, due to the field weakening effect, which necessitates the use of the λ field weakening scaling.

$$G_{TF} = \frac{(K_P s + K_I)K_T\lambda}{Js^2 + Bs + (K_P s + K_I)K_T\lambda} \tag{2}$$

where

$$\lambda = 1 \qquad for\ \omega_r \le \omega_{base}$$
$$\lambda = \frac{\omega_{base}}{\omega_r}\ for\ \omega_r > \omega_{base} \tag{3}$$

The effective torque constant λK_T is unchanged below base speed, ω_{base}, and decreases inversely with the machine speed, ω_r above base speed, as shown in (3). The base speed of the emulator drive system is 9000rpm [11].

The effect of field weakening can also be incorporated into the identified transfer function (1) using λ to take the full operating range into consideration. This transfer function can then be inverted to obtain the corresponding compensator model, (4).

$$G_{comp} = \begin{cases} 1 + \dfrac{0.99s^2 + s}{0.01s^2 + 16s + 1569}, & \omega_r \le 9000rpm \\ 1 + \dfrac{0.99s^2 + s}{0.01s^2 + (16s + 1569)} \cdot \dfrac{\omega_r}{9000}, & \omega_r > 9000rpm \end{cases} \tag{4}$$

4 Experimental Results

In this section, the experimental emulation results of the different inertia systems and the mechanical drivetrain resonant modes are presented. The uncompensated and compensated responses are compared to demonstrate the performance of the new emulation method.

4.1 Emulation of a linear system with different inertias

Normally, provided that the torque rating of the electrical machine is sufficient, the HIL emulation of the mechanical prime mover based on the machine drive should present no problem when the motor inertia is smaller than that of the emulated power source. However, if the prime mover has a high power density and so a much smaller inertia constant, then the electrical drive system emulation performance may be unsatisfactory. In this study, a heuristic investigation on the emulation performance of gas engines of different inertias is performed through the emulation of a generic mechanical equation of motion, (5).

$$G_{em} = \frac{1}{J_{em}s + B_{em}} \tag{5}$$

This generic linear system model is implemented in the simulation environment (RTP) shown in Fig. 2. The emulation capability of (5) with different inertias is examined for steady state and transient conditions. The speed controller G_s has been designed to give a closed-loop bandwidth of 60rad/s for the motor nominal parameters listed in the Appendix and is unchanged throughout the inertia testing. Two linear systems both with inertias less than the emulator system actual inertia of 0.116kgm^2 have been tested with and without the compensator in place. The emulated inertias are 0.0187kgm^2 (low J case) and 0.011kgm^2 (minimum J case) The emulation system speed was set to 11140rpm and the emulation performance was tested by applying a 15kW step up and step down in load power.

Fig. 3(a) and (b) shows the emulation performance for the low inertia case (around 6 times smaller than the actual inertia of the emulation system) when the compensator is active and Fig. 3(c) and (d) shows the corresponding emulation performance for the same condition without the compensator. Without the compensator, a poor speed tracking performance is obtained where a large speed variation is observed in both power step up and step down scenarios. When the actual emulation system inertia is larger than the inertia of the system being emulated, then the emulated dynamics are faster than the drive system and the motor torque-producing requirement may increase. For the low inertia test, the bandwidth of the model speed dynamics is around the resonant peak of the uncompensated drive system. Due to the high gain at the resonant frequency and the high torque requirement, the motor speed controller may saturate, which contributes to the oscillations in both measured speed and torque signals in Fig. 3(c) and (d). When the compensator is enabled, the resonant peak is eliminated and the emulation bandwidth of the test system is extended, which enables excellent dynamic speed tracking, Fig. 3(a) and (b).

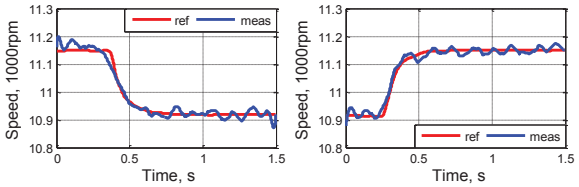

(a) Speed with compensator enabled

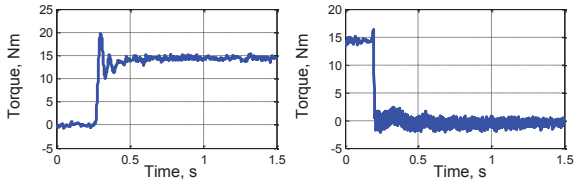

(b) Torque with compensator enabled

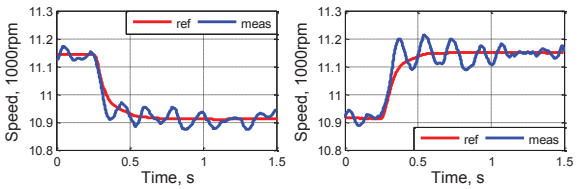

(c) Speed with compensator disabled

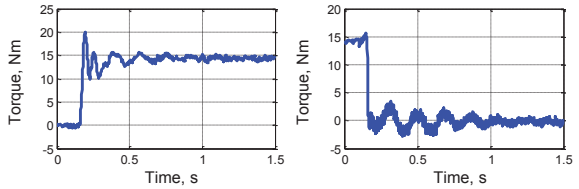

(d) Torque with compensator disabled

Figure 3. Emulation performance for the small inertia system (0.0187kgm^2)

Fig. 4(a) shows the compensator performance for a 0.011kgm^2 inertia value, which is smaller than that in Fig. 3. In this case, a small speed oscillation is visible, which results from the compensator's output exceeding the drive's slew rate (393.68rads^{-2}) as shown in Fig. 4(b). When the emulated inertia is smaller than 0.011kgm^2, the amplitude of the observed oscillation is larger, which indicates that 0.011kgm^2 is the minimum inertia that can be emulated with the system.

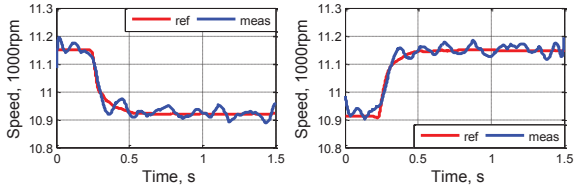

(a) Speed with compensator enabled

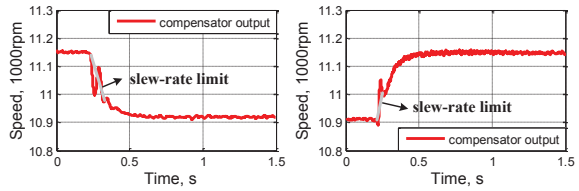

(b) Compensated output speed reference

Figure 4. Emulation performance for the limiting inertia system (0.011kgm^2) with the compensator enabled.

Fig. 5 shows the speed tracking performances of the emulation system for the high inertia case (16 times the inertia of the actual emulation system) with and without the compensator. During the same test condition as in the low inertia case, it takes 9s for the high inertia model speed to reach steady state after a power transient is applied. Such slow dynamics are well within the bandwidth of the uncompensated drive system. Therefore, the compensator is not effective for improving the emulation performance, as the uncompensated system is already capable of emulating the high inertia dynamics on its own.

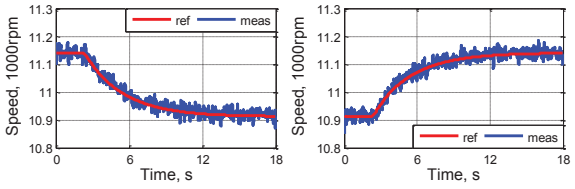

(a) With compensator enabled

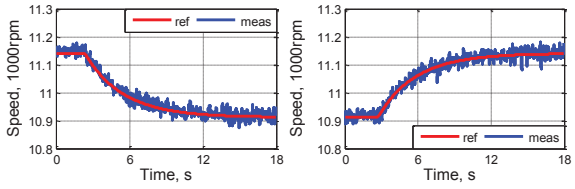

(b) With compensator disabled

Figure 5. Emulation performance for the large inertia system (1.87kgm^2).

4.2 Emulation of an aero mechanical drivetrain system

A mechanical drivetrain is very common in many transportation applications where it is not practical to mount the electrical generator or driven load directly on the prime mover. Fig. 6 shows a simplified generic electro-mechanical system with a non-embedded generator, which can be represented by a reduced order, two-inertia mechanical drivetrain model. This model can be tuned for different natural resonant frequencies, and it is these natural resonant frequencies, which, if excited, may lead to fatigue in mechanical components and instability in the electrical network [12]. Therefore the capability of a HIL emulation system to reproduce the relevant resonant modes in the drivetrain enables the future investigation of electro-mechanical interactions between the prime mover and generator.

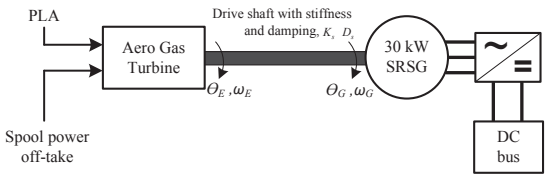

Figure 6. Aero engine electro-mechanical system.

A simple aero mechanical drivetrain model can be obtained by combining the lumped inertias of auxiliary loads and the torsional stiffness of all driveshafts, leaving a two inertia system, which is dominated by the inertias of the engine spool and the aero generator and the stiffness of a common driveshaft [12]. The engine inertia, J_E, in the drivetrain model is 1.87kgm^2. The generator inertia, J_G, driveshaft stiffness, K, and the viscous damping, D, are varied to give the emulated resonant frequency based on (6). In practice, the mechanical drivetrain will have multiple resonant modes, which could be emulated by a more detailed mechanical model. For illustrative purposes, this paper considers a single tunable mode model, shown in Fig. 7, which can be determined from Fig. 6.

$$f_n = \sqrt{K\left(\frac{1}{J_E}+\frac{1}{J_G}\right)} \tag{6}$$

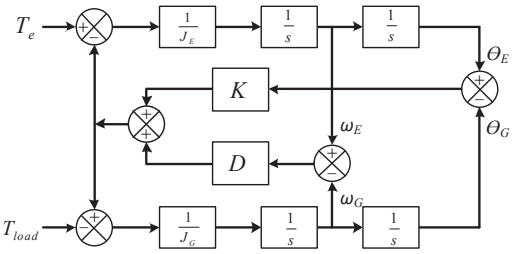

Figure 7. Mechanical drivetrain emulation model.

The results for the drivetrain emulation are presented in Figs. 8 to 11. Two different resonant modes (12Hz and 18Hz), which are within the drivetrain resonant frequency range identified in a similar hardware test system [12], are emulated with and without the compensator enabled. The speed controller in the emulation drive system again has a 60rad/s bandwidth. In order to excite the drivetrain resonances, an external power step 15kW is applied when the machine is running at the steady-state speed of 9000rpm.

Figs. 8 and 9 show the compensator performance for the emulation of a low frequency resonant mode (12Hz). In this case study, the generator inertia J_G is 0.05kgm^2, the driveshaft damping D is 0.2Nmsrad^{-1} and the shaft stiffness K is set to 263Nmrad. Fig. 8(a) shows the measured speed transient during the power step up in comparison with the speed reference from the drivetrain model and Fig. 8(b) is the corresponding measured torque transient. In Fig. 8(a), it is quite difficult to differentiate the real motor speed due to a wide range of low frequency noise. However, a periodic variation at the resonant frequency can be easily identified in the torque transient in Fig. 8(b).

In order to demonstrate the effectiveness of the emulation compensator, a frequency analysis using fast Fourier transform (FFT) is performed on both the speed and torque transients. Fig. 8(c) compares the measured motor speed transient and the model reference output in the frequency domain for the 0.7s time period after the electrical load step is applied. In Fig. 8(c), a very strong resonant frequency at 12Hz is clear in the speed reference, which suggests a correct torsional speed oscillation was triggered by the power step. Such a speed variation is attenuated very quickly by the system damping, as shown in Fig. 8(a). In Fig. 8(c), the 12Hz resonant mode is also present in the measured motor speed

FFT. However, there is a second peak at 17Hz, which is not present in the reference speed. This frequency is believed to belong to the low frequency noise.

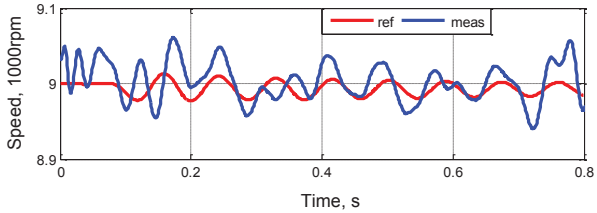

(a) Speed time domain data

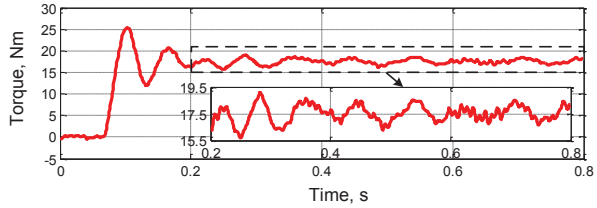

(b) Torque time domain data

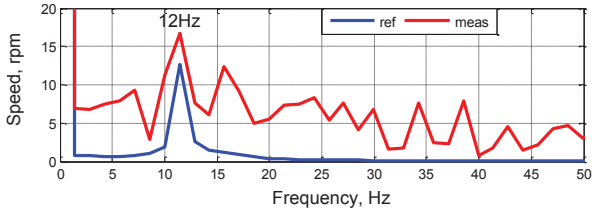

(c) FFT of the speed transients

Figure 8. Key waveforms for the resonant mode of 12Hz in the mechanical drivetrain with the compensator enabled.

Fig. 9 allows the torque transient response of the compensated and uncompensated 12Hz resonant mode model to be compared. The 0.7s time duration is chosen to be the same as that in the speed FFT analysis for a fair comparison. When the compensator is employed, a frequency at 12Hz is identified, which is the excited drivetrain resonance, however, when the compensator is disabled, the emulator is unable to follow the 12Hz resonance which is as expected, since the uncompensated system is tuned for around 10Hz. Based on these results the HIL emulation with compensator is able to introduce the correct frequency of resonance exhibited by a high order system such as a mechanical drivetrain, but with some variation in magnitude. Since the resonance magnitude depends on damping, it is hard to obtain accurately.

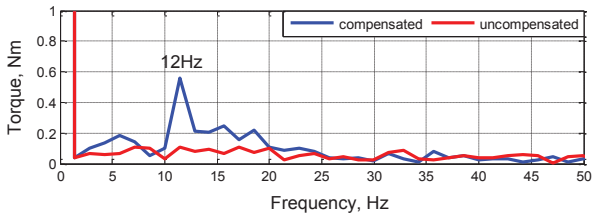

Figure 9. FFT of 12Hz resonance torque transients for the 0.7s time window after the electrical power step.

Figs. 10 and 11 show the compensator performance for the emulation of a high frequency resonance (18Hz) when excited by a 15kW load step. In this case, the driveshaft stiffness K is increased to 634Nmrad in order to get the emulated resonance. All spectrum analysis is performed over the same 0.7s time window as the low frequency resonance test. As in Fig. 8(a), the measured speed is corrupted by a variety of low frequency noise in Fig. 10(a), so the 18Hz frequency in the reference signal is not identifiable. The FFT analysis of the speed transients in Fig. 10(c) shows two main peaks at 6Hz and 18Hz respectively. The peak at 18Hz is the emulated mode, which is triggered by the load step. This frequency has a peak of 18rpm that is lower than the reference of 26rpm in Fig. 10(c), which is as expected, since the resonant mode is beyond the 15.9Hz cut-off frequency of the compensator. The other frequency at 6Hz is attributed to the slew rate limit effect where the compensator output exceeds the drive's inherent slew rate. The torque FFT analysis in Fig. 11 for the compensated system also gives peaks at 6Hz and 18Hz which correspond to the peaks in the speed FFT. The identified resonances in the spectrum analysis can also be observed in the torque transient, Fig. 10(b).

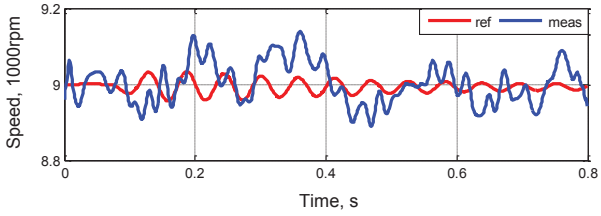

(a) Speed time domain data

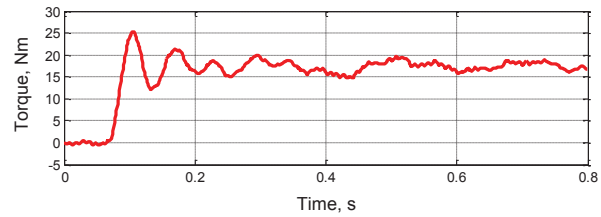

(b) Torque time domain data

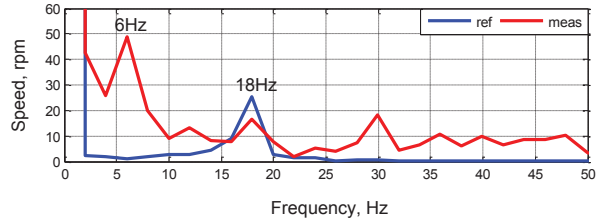

(c) FFT of the speed transients

Figure 10. Key waveforms for the resonant mode of 18Hz in the mechanical drivetrain with the compensator enabled.

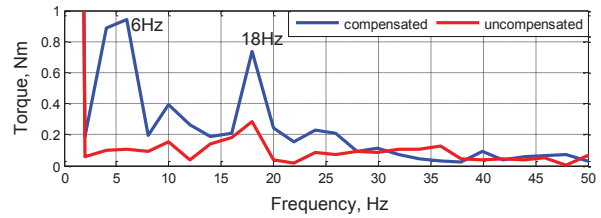

Figure 11. FFT of 18Hz resonance torque transients for the 0.7s time window after the electrical power step.

The high frequency resonance emulation is beyond the bandwidth of the compensator and affects the compensator's performance. However, in comparison to the uncompensated test, the compensator still allows the emulated resonance to occur although the emulated resonance peak is attenuated. The results presented in Figs. 8 to 11 have demonstrated the effectiveness of the developed compensator in the high order system resonances emulation.

5 Conclusion

This paper has presented a drive system compensator, which is valid over the full power speed envelope for a bandwidth up to 100rad/s. The developed compensator can be easily designed and implemented without accurate knowledge of the system parameters. The compensator enables accurate HIL emulation of a wide range of high speed and high power prime movers without the need to redesign the emulation controller.

The effectiveness of the proposed compensator design has been demonstrated through the experimental emulation of different inertia systems with 0.011kgm^2 (approx. 1/10 the test system) being identified as the minimum inertia which can be emulated correctly. Drivetrain resonant modes up to the bandwidth limit of the compensator (15.9Hz) have also been correctly emulated. The emulation results show very good correspondence between the model output and the measured drive speed, which confirm that the compensator can extend the emulation capability of the uncompensated system. Limits of the emulation method have been identified, which are related to both the bandwidth of emulated dynamics and the electrical drive inherent slew rate limit. The slew rate limit could be increased by using a converter with a higher current rating, up to the thermal and saturation limit of the induction motor, but could increase the system cost. Increasing the machine rating could increase both torque and inertia, giving at most marginal gains on slew rate and hence compensator performance.

Acknowledgements

The authors would like to acknowledge the studentship support from The University of Manchester Alumni Fund and the School of Electrical and Electronic Engineering, and to thank Rolls-Royce plc for promoting and funding the Intelligent Electrical Power Network Evaluation Facility (IEPNEF).

References

[1] X. Roboam, B. Sareni, and A. D. Andrade, "More Electricity in the Air: Toward Optimized Electrical Networks Embedded in More-Electrical Aircraft," *IEEE Industrial Electronics Magazine*, vol. 6, pp. 6-17, 2012.

[2] K. L. Lian and P. W. Lehn, "Real-time simulation of voltage source converters based on time average method," *IEEE Trans. Power Syst*, vol. 20, pp. 110-118, Feb. 2005.

[3] A. Mackay, S. Galloway, C. Booth, and J. R. McDonald, "Real-time assessment of relay protection schemes on integrated full electric propulsion systems," in *Proc. IEEE Electr. Ship Technol. Symp.*, pp. 230-236, 2005.

[4] R. Todd and A. J. Forsyth, "HIL emulation of all-electric UAV power systems," in *Proc. of IEEE Energy Conversion Congress and Exposition (ECCE)*, pp. 411-416, 2009.

[5] B. A. Correa, Y. Zhang, R. Fang, and R. A. Dougal, "Driving a synchronous motor so that it emulates a twin-shaft gas turbine engine," in *Pro. of the 6th IET Power Electronics, Machines and Drives (PEMD) conference*, Mar.26-29, 2012.

[6] H. M. Kojabadi, L. Chang, and T. Boutot, "Development of a novel wind turbine simulator for wind energy conversion systems using an inverter-controlled induction motor," *IEEE Trans. Energy Conv*, vol. 19, pp. 547-552, 2004.

[7] B. A. Correa, Y. Zhang, R. A. Dougal, T. Chiocchio, and K. Schoder, "Mechanical Power-Hardware-in-the-Loop: Emulation of an Aeroderivative Twin-Shaft Turbine Engine," in *Proc. of IEEE Electric Ship Technologies Symposium (ESTS)*, pp. 464-468, 2013.

[8] L. A. C. Lopes, J. Lhuilier, and M. F. Khokhar, "A wind turbine emulator that represents the dynamics of the wind turbine rotor and drive train," in *Proc. of IEEE Power Electronics Specialists Conference (PESC)*, pp. 2092-2097, 2005.

[9] B. Rabelo, W. Hofmann, and M. Gluck, "Emulation of the static and dynamic behaviour of a wind-turbine with a DC-machine drive," in *Proc. of IEEE Power Electronics Specialists Conference (PESC)*, pp. 2107-2112, 2004.

[10] Z. Hakan Akpolat, G. M. Asher, and J. C. Clare, "Dynamic emulation of mechanical loads using a vector-controlled induction motor-generator set," *IEEE Trans. Ind. Electron*, vol. 46, pp. 370-379, 1999.

[11] C. Gan, "Enabling technologies for next generation aircrafts," PhD thesis, School of Electrical and Electronic Engineering, The University of Manchester, UK, 2014.

[12] T. Feehally, "Electro-mechanical interaction in aero gas turbine-generator systems for more-electric aircraft," PhD thesis, School of Electrical and Electronic Engineering, The University of Manchester, UK, 2012.

Appendix

Table I: Nominal parameters of the emulation facility

Parameter	Value
Test rig inertia (±10%), J	0.116Kgm^2
Test rig damping ratio, B	0.0018Nms
Machine torque constant, K_T	0.85Nm/A
Speed controller proportional gain, K_P	4.5
Speed controller integral gain, K_I	270
Current controller proportional gain, K_{PI}	36
Current controller integral gain, K_{II}	116